

Structural Studies on Bioactive Compounds. 30. Crystal Structure and Molecular Modeling Studies on the *Pneumocystis carinii* Dihydrofolate Reductase Cofactor Complex with TAB, a Highly Selective Antifolate^{†,‡,§}

Vivian Cody,^{*,||} David Chan,[⊥] Nikolai Galitsky,^{||} Dawn Rak,^{||} Joseph R. Luft,^{||} Walter Pangborn,^{||} Sherry F. Queener,[#] Charles A. Laughton,[⊥] and Malcolm F. G. Stevens[⊥]

Hauptman-Woodward Medical Research Institute, Inc., 73 High Street, Buffalo, New York 14203, Department of Pharmacology and Toxicology, Indiana University School of Medicine, Indianapolis, Indiana 46202, Cancer Research Laboratories, School of Pharmaceutical Sciences, University of Nottingham, Nottingham, U.K. NG7 2RD

Received October 22, 1999; Revised Manuscript Received January 24, 2000

ABSTRACT: The crystal structure of the ternary complex of NADPH, the potent antifolate [2,4-diamino-5-{3-[3-(2-acetyloxyethyl)-3-benzyltriazen-1-yl]-4-chlorophenyl}-6-ethylpyrimidine] (TAB, **1**) and *Pneumocystis carinii* dihydrofolate reductase (pcDHFR), refined to 2.1 Å resolution, reveals that TAB binds similar to the antifolates trimethoprim and methotrexate. These data also reveal multiple conformations for the binding geometry of TAB with two preferred orientations of the acetyloxy and benzyl groups that results from a 180° rotation about the N2–N3 triazenyl bond. The methyl of the acetyloxy and benzyl ring of TAB probes large hydrophobic regions of the *p*-aminobenzoyl folate binding pocket of the active site, in particular the region near Phe69, which is unique to the pcDHFR sequence. These results confirm prior molecular modeling investigations of the binding of TAB to pcDHFR that identified four low-energy binding geometries, two involving rotations about the terminal N(2)–N(3) triazenyl linkage and two involving atropisomerism about the pivotal pyrimethamine–phenyl bond. The primary differences in the molecular dynamics (MD) models and those observed in this crystal complex result from small conformational changes in active-site residues on energy minimization. However, two MD models place the acetyloxy and benzyl ring groups in a region of the active site between the cofactor-binding region and the *p*-aminobenzoyl folate pocket; an orientation never observed in any DHFR crystal structure to date. These conformers interact with solvent near the enzyme surface and are probably not observed due to the loss of specific hydrogen bonds with the enzyme. The high species pcDHFR selectivity of TAB could be the result of ligand flexibility that enables multiple binding orientations at the enzyme active site. Further modification of the acetyloxy region of TAB could increase its potency and selectivity for pcDHFR.

The opportunistic fungal infection *Pneumocystis carinii* (pc) elicits a pneumonia (PCP),¹ which has been recognized as a major cause of morbidity and mortality in HIV-positive patients (1, 2). Current treatment of the disease with dihydrofolate reductase (DHFR) inhibitors such as the antifolate trimethoprim is only moderately successful (3). The inherent lack of potency and selectivity toward the

microbial enzyme necessitates combination therapy with a sulfonamide to achieve the desired therapeutic effect, and severe adverse reactions often precipitate discontinuation of therapy. Recently, trimetrexate **2** (Figure 1), which is 1500 times more potent an inhibitor of pcDHFR than trimethoprim, has been evaluated in PCP treatment (4). The higher potency removes the need for an additional sulfonamide, but its lack of species selectivity introduces a new problem. Expensive concomitant folate rescue therapy with leucovorin is required to ameliorate undesirable host toxicity. For these reasons, the design and synthesis of agents that possess both potency and species specificity toward pcDHFR has been the focus of much recent research effort (5–10).

Among the various classes of antifolates designed to have increased pcDHFR selectivity, bicyclic analogues to 2,4-diaminopteridines have received the most attention in recent years. Notably, novel furo[2,3-*d*]pyrimidines are more selective than 5-deazapteridine nonclassical analogues (6, 7) or pyridopyrimidines (8). The lipophilic furopyrimidine analogue, 2,4-diamino-5-[(2-naphthylthio)-methyl]furo[2,3-*d*]pyrimidine (MTOS, **3**), shows the highest selectivity for

[†] Supported in part by GM-51670 (V.C.), N01-AI-35171 (S.F.Q.), and the Cancer Research Campaign, U.K. (M.F.G.S., C.A.L., and D.C.).

[‡] Protein data bank tracking number: RCSB 009895

[§] Paper 29: Hannah, D. R., Sherer, E. C., Laughton, C. A., Davis, R. V., Titman, R. B., and Stevens, M. F. G. (2000) *Bioorg. Med. Chem.* (in press).

* To whom correspondence should be addressed. E-mail: cody@hwi.buffalo.edu. Fax: (716) 852-6086.

^{||} Hauptman-Woodward Medical Research Institute, Inc.

[#] Department of Pharmacology and Toxicology.

[⊥] Cancer Research Laboratories.

¹ Abbreviations: pcDHFR, *Pneumocystis carinii* dihydrofolate reductase; TAB, 2,4-diamino-5-{3-[3-(2-acetyloxyethyl)-3-benzyltriazen-1-yl]-4-chlorophenyl}-6-ethylpyrimidine; MD, molecular dynamics; TMP, trimethoprim; MTX, methotrexate; NADPH, nicotinamide diphosphate adenine ribose; MTOS, 2,4-diamino-5-[(2-naphthylthio)-methyl]furo[2,3-*d*]pyrimidine; PCP, *pneumocystis carinii* pneumonia.

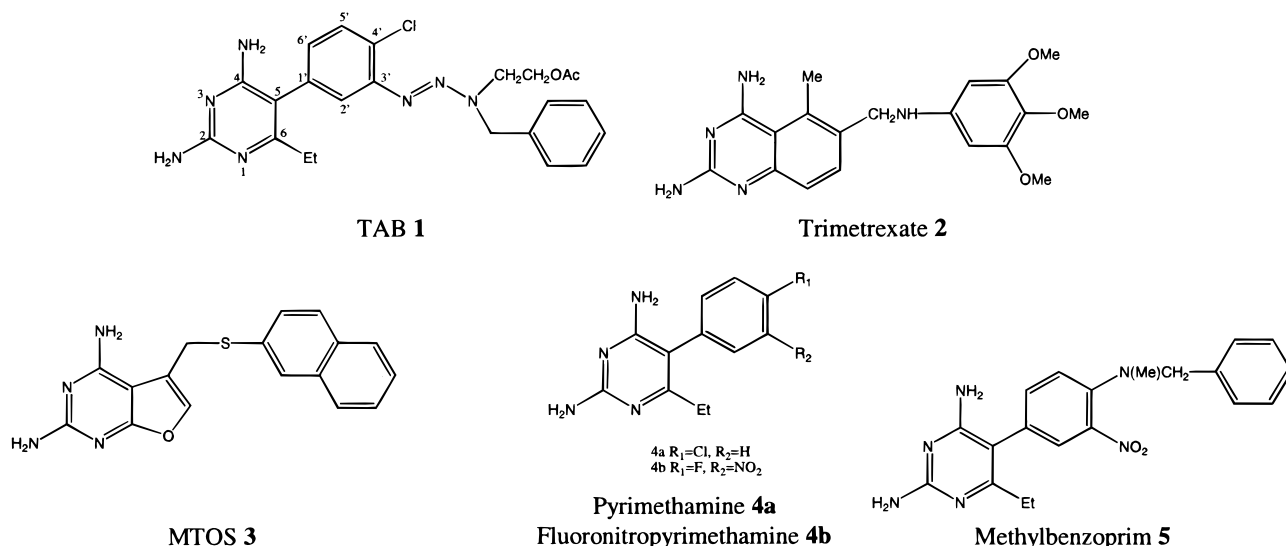


FIGURE 1: Schematic representation of the structures of TAB 1, trimetrexate 2, MTOS 3, pyrimethamine 4a, fluoronitroypyrimethamine 4b, and methylbenzoprim 5.

pcDHFR in this series of analogues studied and has a selectivity ratio of rat liver to pcDHFR of 18.9 (9).

Although monocyclic 2,4-diaminopyrimidines such as trimethoprim and pyrimethamine (4a, Figure 1) are only weakly inhibitory against pcDHFR, modification of these starting structures has led to improved potency. Structure-activity data for a series of triazene-substituted 2,4-diaminopyrimidines showed that one compound, TAB 1, a triazene-substituted analogue of pyrimethamine 4a (Figure 1), is the most pc-selective antifolate yet reported with an IC_{50} of 0.17 μ M for pcDHFR and a selectivity ratio between rat liver and pcDHFR of 114 (10).

At the time when TAB was tested for activity against pcDHFR, there was no accurate three-dimensional structural information on the target enzyme available (10). The availability of X-ray ternary complex structures for pc and human DHFR enzymes (PDB code 1dyr and 1dls) (11) has prompted us to engage in a program of lead optimization. Sequence and structural alignment of pcDHFR with the human enzyme reveals that their folate-binding sites are highly conserved with few significant differences. There are only six nonidentical residues: the most interesting features are that Lys37 and Phe69 in pcDHFR replace the corresponding human enzyme residues Gln35 and Asn64. Phe69, together with residues Ile33, Phe36, Pro66, and Leu72, form a hydrophobic pocket, and compounds which interact favorably with Lys37 and/or Phe69 could thus provide species selectivity.

Molecular modeling and structure-based design methods have been used to analyze the conformation of ligands with diverse structures in the pcDHFR active site (12–14). Docking studies using molecular dynamics simulations of the binding of N(5)-deazapterin antifolates by Gorse revealed that the substrate-binding site of human DHFR has sufficient space to host ligands in a variety of different orientations (14).

We envisaged that the generous proportions of the active site of the pcDHFR enzyme could allow suitable ligands to bind in multiple conformations. The lead compound TAB displays several interesting structural features: the N(1)=N(2) double bond in triazenes, like that in azo-compounds,

is fixed in the trans geometrical configuration; there is restricted rotation about the N(2)–N(3) triazene bond because the terminal N(3) atom in triazenes displays considerable sp^2 character (15, 16); and finally, like the comparable phenomenon in biphenyls (17, 18), the pivotal pyrimidine-phenyl bond in TAB is restricted from free rotation (atropisomerism) because of the flanking substituents in the diaminopyrimidine moiety and the buttressing effect which the triazene group exerts on the 2'-H atom in the 5-phenyl residue. We reasoned that TAB might exhibit multiple-binding conformations when interacting with the pcDHFR enzyme. In support of this proposal, Tendler and colleagues have shown by [19 F]NMR that both atropisomers of fluoronitroypyrimethamine 4b can bind to *Lactobacillus casei* DHFR (binary complex) with different affinities (19). Also, 1 H NMR studies on the binding of methylbenzoprim 5 to this enzyme as a ternary complex with NADP $^+$ confirmed that the drug can adopt multiple binding conformations at the active site (20).

Structural data for human and pcDHFR inhibitor complexes have been carried out for a number of antifolates including trimethoprim (21), methotrexate, and folate (22), as well as number of novel fuopyrimidine classical and nonclassical antifolates (9, 23). These data show that the key structural features of the active site are conserved although there are a number of residue changes with the active site, namely in pcDHFR, there is a change from the human sequence of Phe31 to Ile33, Gln35 to Lys37, and Asn64 to Phe69. Comparison of these structures reiterates the role of selective inhibitor interactions with these mutational sites to enhance selectivity between human and pcDHFR. These data also show that the volume of the active site is slightly smaller in the pcDHFR enzyme than human and that these small changes can enhance binding affinity and thus selectivity for one enzyme over the other.

We report the use of molecular modeling techniques to predict the binding conformation of TAB to pcDHFR. We also confirm the validation of the modeling studies by the determination of the crystal structure of a pcDHFR ternary complex with cofactor NADPH and TAB refined to a resolution of 2.1 Å. The crystal data has revealed multiple

Table 1: Crystal Properties and Refinement Statistics for pcDHFR TAB NADPH Complex

lattice constants (Å)	37.481, 43.137, 61.288, $\beta = 94.74$		
space group	$P2_1$		
resolution range (Å)	8.0–2.1		
reflections used	10 325		
R factor (%)	19.0		
protein atoms	1678		
water molecules	65		
B factor (protein average) (Å ²)	24.34		
R_{merge} (%)	6.9		
completeness (2.18–2.10 Å)	97.8		

targets		root-mean-square deviation	
distances (Å)			
main-chain bond (1.750)	1.564	bonds (0.020)	0.020
main-chain angle (2.500)	2.378	angles (0.040)	0.065
side-chain bond (1.750)	1.641	planar 1–4 (0.050)	0.081
side-chain angle (2.500)	2.426	planar (0.020)	0.016
chiral restraint (0.150)	0.228	planar group (0.02)	0.013
nonbonded distances		chiral volume (0.5)	0.220
single torsion (0.500)	0.229	torsion angles, degrees	
multiple torsion (0.50)	0.313	planar (3.0)	2.4
hydrogen bonds (0.50)	0.334	staggered (15.0)	23.6
		orthonormal (15.0)	25.9

conformational modes of binding for TAB, as the modeling studies predicted. These data provide insight into the possible origins of the selectivity of TAB for pcDHFR over human DHFR.

EXPERIMENTAL SECTION

Crystallization and X-ray Data Collection. Recombinant pcDHFR was cloned, isolated, and purified as previously described (24). The protein was washed in a centricon-10 three times with 50 mM Mes buffer at pH 6.0, 100 mM KCl buffer, and concentrated to 14.3 mg/mL. A novel thermal gradient technique (25, 26) was used to carry out the crystallization screens with pcDHFR. Crystallization of the pcDHFR–TAB complex was carried out by adding 10 μ L of protein, 3 μ L of Mes/KCl buffer, and 7 μ L of 50% (w/v) PEG2000 in 50 mM Mes, pH 6.0, and 100 mM KCl and placing the mixture in a capillary for equilibration on a thermal gradient apparatus. Samples of pcDHFR were also incubated with NADPH along with TAB and incubated overnight at 4 °C. The protein was washed to remove excess inhibitor and cofactor and concentrated to 9.8 mg/mL. This sample was set up with 40% (w/v) PEG 2000 with 50 mM Mes buffer, pH 6.0, and placed in the thermal gradient device.

Data collection was carried out at room temperature on the best crystal available to 2.1 Å resolution using a Rigaku RaxisIIc Imaging plate system with a rotating anode source. Diffraction data showed a monoclinic lattice, space group $P2_1$ with cell parameters $a = 37.481$, $b = 43.137$, $c = 61.266$ Å, and $\beta = 94.74^\circ$ for the ternary complex. Crystal lattice properties and data collection statistics are listed in Table 1.

Structure Determination and Refinement. The initial structure of pcDHFR–NADPH–TAB complex was solved by molecular replacement methods using the protein coordinates from the ternary complex of the furopyrimidine pcDHFR complex (23), minus the cofactor and inhibitor atoms, with the restrained least-squares program PROLSQ (27, 28); (modified by G. D. Smith, HWI) in combination with the model-building program CHAIN (29). All calculations

were carried out on a Silicon Graphics Impact R10000 Workstation. The initial $(2|F_o| - |F_c|)\exp i\alpha c$ maps, where F_o is the observed and F_c the calculated, structure factors based on the protein model only, and αc is the calculated phase, resulted in electron density corresponding to both the inhibitor TAB and the cofactor, NADPH, as well as a good fit of the protein to its density.

Further restrained refinement was continued for the ternary complex, including the cofactor and inhibitor. A model of TAB was generated from the crystal structure of the 3'-triazenyl dimethyl derivative (10) and optimized with Sybyl (30). NADPH was taken from the pcDHFR MTXO ternary structure (23). The aromatic rings of TAB and NADPH were constrained to be planar. Between least-squares minimizations, the structure was manually adjusted to fit difference electron density and verified by a series of OMIT maps calculated from the current model with deleted fragments.

Interpretation of the electron density in the active site revealed that the inhibitor could be fit with the triazenyl substitute in alternative orientations (Figure 2). The final refinement was carried out with a 50% population of the conformers that result from an 180° rotation about the N(2)–N(3) triazenyl bond. The thermal parameters for these atoms were consistent with this distribution. Electron density near the pyrimidine 6 position was difficult to interpret as the elongated density had partial overlap with the position of the conserved water that interacts with Glu32 and Trp27 and is observed in all structures. A final disorder model was used to fit this region.

The final refinement statistics are summarized in Table 1. The Ramachandran conformational parameters from the last cycle of refinement generated by PROCHECK (31) shows that 87% of the residues have the most favored conformation and none are in disallowed regions. Coordinates for this structure have been deposited with the Protein Data Bank (tracking no. RCSB 009895).

Molecular Modeling. Computational Methods. Since the molecular-modeling studies were carried out prior to this structure determination, coordinates for pcDHFR were taken from the Brookhaven Protein Data Bank (11), 1dyr (21). MOPAC (32) with AM1 Hamiltonian (33) was used to calculate the ESP charges (34) and to optimize TAB and molecular mechanics energies were minimized before docking in the enzyme active site. A formal charge of +1 was assigned to the N1 atom of pyrimidine. The starting conformation was achieved by least-squares superimposition of the 2,4-diaminopyrimidine moiety of TAB onto that of trimethoprim.

Manual Docking Studies. The molecular modeling software INSIGHT II 95 (35) provides an interface to the AMBER 3.5 force field (36). Unfavorable contacts (0.3% overlap of van der Waals radii) were removed manually by adjusting the position of TAB and the enzyme amino acid side chains. Several cycles of minimization steps and manual removal of unfavorable contacts were carried out until no further changes occurred.

Molecular Dynamics (MD) Studies. All calculations were implemented using the AMBER 4.1 suite of software (37) with the Cornell et al. all-atom force field model (38) on a R10000 Silicon Graphics Indigo workstation. Molecular mechanics parameters required for NADPH and TAB are

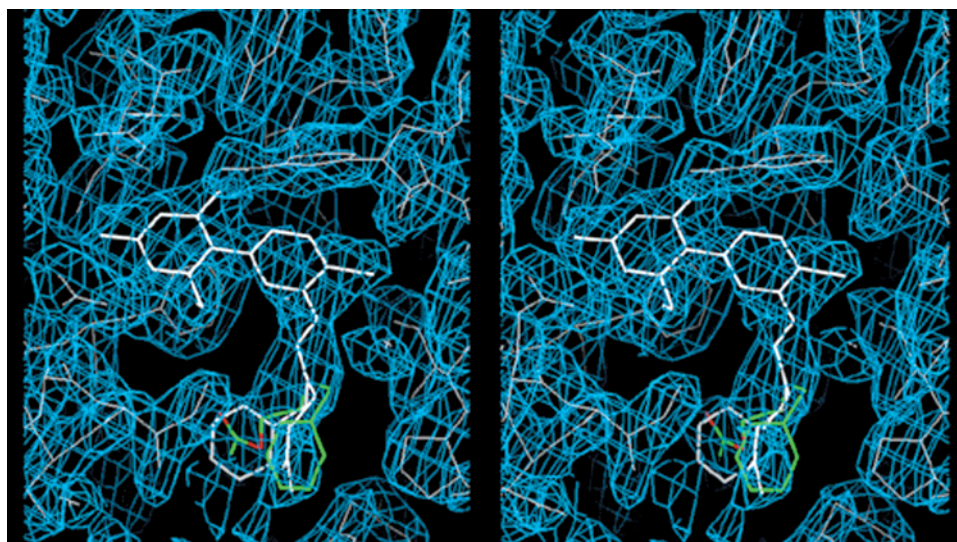


FIGURE 2: Difference electron density ($2F_o - F_c$, 0.8σ) showing the fit of TAB in two alternative orientations for the benzyl and acetyloxy groups.

not present in the default AMBER force field. All the necessary parameters for NADPH were taken from ab initio quantum mechanical calculations performed by Leach and Klein (39). Structural and atomic partial charge parameters for TAB were constructed using X-ray crystallographic data from a close analogue, dimethyltriazenyl pyrimethamine (10), followed by energy minimization at the semiempirical AM1 level (34) as described earlier. All the MD simulations received the following treatment. Dynamics runs were of 100 ps in length and had a time step of 2 fs. The SHAKE (40) algorithm was used to constrain bond lengths at their equilibrium values. Each run was initiated with a new random number seed. The standard AMBER van der Waals terms was replaced by a “soft repulsion” potential. The AMBER “soft-repulsion” energy term, E , has the following characteristic:

$$E = K_{\text{rep}}(r_o^2 - r^2)^2, r < r_o$$

$$E = 0, r > r_o$$

where K_{rep} is a force constant ($1 \text{ kcal mol}^{-1} \text{ \AA}^{-4}$ in this study) and r_o is the sum of the van der Waals radii of the two interacting atoms. Electrostatic potential was varied according to the changes of the soft repulsion potential. In the beginning of the dynamics run, K_{rep} was set at 1 kcal/mol/\AA^4 . It was then scaled down linearly to 0 over a time scale of 10 ps at 5 ps into the run. The electrostatic interactions remained on in the first 7 ps, it was then scaled down linearly and was completely switched off at 15 ps. Both the “soft” nonbonded (K_{rep}) and electrostatic terms remained at zero during the holding phase of the dynamics run. To coincide with the slow cooling phase of the annealing run, both terms were scaled up linearly over a 25 ps period. A dynamic zone of 8 \AA radius from TAB was created with atoms frozen outside this zone. The nonbonded cutoff was 8 \AA . A distance-dependent dielectric constant ($\epsilon = r_{ij}$) was used to model solvent effects, as the inclusion of explicit solvent is computationally inefficient and incompatible with simulated annealing method, which requires high temperature dynamics (water molecules “boil off”). Distance restraints were

introduced to maintain hydrogen bonds contacts between the amino groups of TAB and Ile10, Glu32, and Ile144. Heavy atoms of NADPH, Glu32, and the 2,4-diaminopyrimidine moiety of TAB were also positionally restrained. Dynamics calculations were implemented in stages using the SANDER module of AMBER. All systems were energy minimized to an rms gradient of $<0.1 \text{ kcal/mol/\AA}$ before and after dynamics runs by using a combination of steepest descent and conjugate gradient methods. The simulated annealing protocol itself consisted of three phases—heating, holding, and slow cooling. At the beginning and the end of annealing were two 5 ps relaxation stages at 1 K. The 10 ps heating phase brought the temperature of the system linearly to 750 K. TAB was allowed to explore its conformational space for the next 50 ps. The temperature was then decreased linearly to 1 K over the next 35 ps.

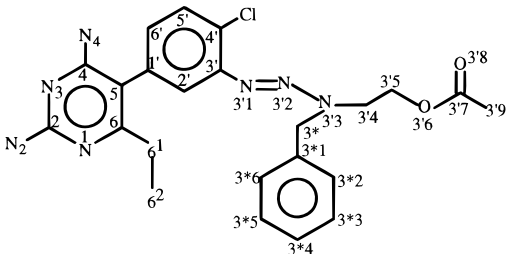
RESULTS

Crystallography. Overall Structure. The structure of pcDHFR TAB ternary complex is similar to that observed for other antifolate complexes (21–23). There is also a cis peptide linkage between Arg67 and Pro68 and Gly124 and Gly125, as observed in other pcDHFR complexes.

Inhibitor Binding. The binding orientation of the pyrimidine ring of TAB is similar to that observed for pcDHFR trimethoprim ternary complex (21), although the plane of the pyrimidine ring is tilted about 17° toward the *p*-aminobenzoyl folate-binding site. The plane of the TAB pyrimidine ring lies on the same plane as that observed for folate (22). The carboxylate oxygen atoms of Glu32 interact with the pyrimidine ring, forming hydrogen bonds by OE2 and OE1 to N(1) and 2-amino group. In addition, the carboxylate oxygens of the glutamate form hydrogen bonds to a conserved Thr144 and to conserved structural water. The 2,4-diaminopyrimidine ring of TAB interacts with Glu32 in the same manner as other antifolates (21–23) and the *p*-chlorophenyl ring torsion angle is near 60° (Table 2), similar to that observed in the crystal structure of the pyrimethamine precursor antifolate (10).

The most notable feature of the binding orientation of TAB in this pcDHFR ternary complex is that the antifolate binding

Table 2: Comparison of the TAB Geometry Based on Crystal Structure and Molecular Dynamics Data



torsion angle	X-ray conf-1	X-ray conf-2	MD rotomer 1	MD rotomer 2	MD rotomer 3	MD rotomer 4
C6–C5–C1'–C2'	62.3	62.3	58.0	58.8	–46.4	–42.7
C5–C6–C61–C62	109.3	109.3	–107.7	75.9	109.4	–62.8
C2'–C3'–N3'1–N3'2	–1.4	–178.6	4.1	–151.3	–179.7	21.7
C3'–N3'1–N3'2–N3'3	–139.1	–140.4	–166.4	171.6	–164.3	167.9
N3'1–N3'2–N3'3–C3*4	15.3	–142.4	178.4	–162.8	28.4	33.4
N3'2–N3'3–C3*4–C3*5	–88.5	–117.7	82.7	131.3	133.3	131.9
N3'2–N3'3–C3*4–C3'5	–71.6	118.8	73.8	177.7	161.4	93.4
N3'3–C3'4–C3'5–O3'6	179.8	–151.6	169.0	70.4	74.0	–166.3
C3'4–C3'5–O3'6–C3'7	–127.3	–145.4	–177.6	166.2	–175.8	177.5
C3'5–O3'6–C3'7–O3'8	5.1	–175.5	–91.3	101.9	–82.6	–43.6

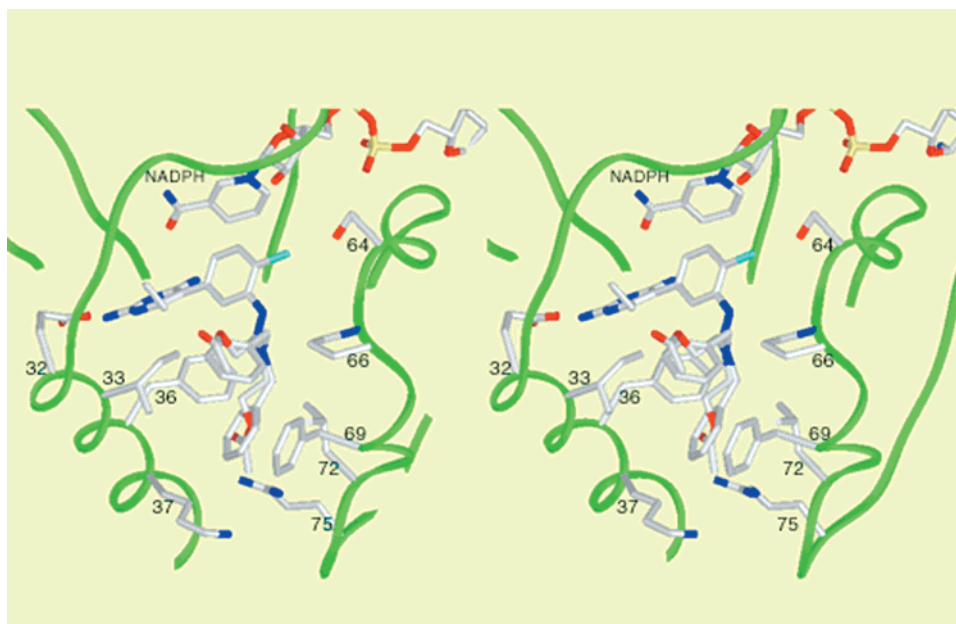


FIGURE 3: Illustration of the fit of the two conformers of TAB in the active site of pcDHFR. The protein backbone is shown as ribbons (green) with TAB and NADPH heteroatoms colored O (red), N (blue), Cl (green), and P (yellow). SETOR program used to create figure (41). Highlighted are the side chains of Glu32, Ile33, Lys37, Ser64, Phe69, and Arg75.

is disordered such that there are two alternative positions for the binding of the benzyl and acetyloxy groups. As illustrated (Figure 2), TAB can be fit to the electron density with two binding orientations that results from rotation about the N2–N3 triazenyl bond. One conformer places the benzyl ring between the hydrophobic regions near Phe36, Leu72 and the methylene carbons of Lys37 while the acetoxy methyl occupies a hydrophobic region near Ile33, Phe69, and Pro66 (Figure 3). An alternative orientation has the benzyl group situated near Ile33, Pro66, and Phe69 with the acetoxy group carbonyl near Lys37 and its methyl group near Leu72. While the benzyl ring occupies hydrophobic pockets in both orientations, there are no direct hydrogen bonds involving the keto function of the acetyl group, except through water mediation.

Molecular Modeling. Manual Docking Studies. Several molecular modeling studies have been used to aid in the identification of key enzyme residues that confer species selectivity to pcDHFR (12–14). Prior to the determination of this crystal structure, manual docking studies of TAB bound to pcDHFR were carried out using the structural data for the ternary complex with trimethoprim and NADPH (21). Initially, the pyrimidine ring of TAB was superimposed on that of trimethoprim, and the remaining flexible units of TAB then manually adjusted to fit the active site. On the basis of this modeling, a hydrophobic contact between the benzyl moiety of TAB and Phe69 of pcDHFR was identified. A conformation in which the two aromatic moieties interacted in a face-edge manner, as commonly observed in protein–ligand complexes, could be achieved. This interaction

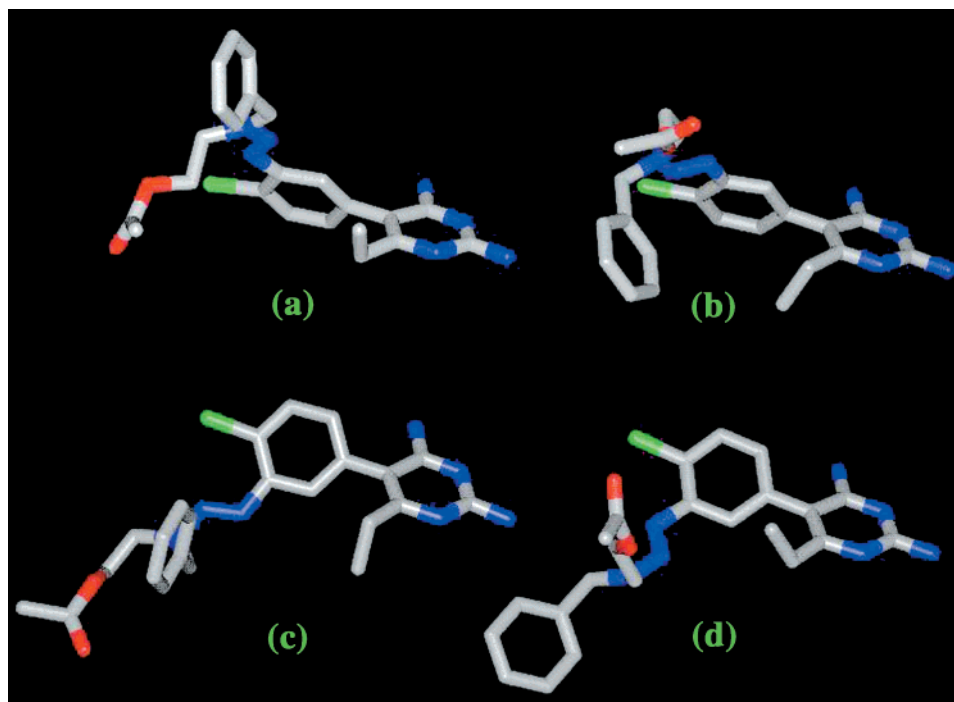


FIGURE 4: The four rotameric forms of TAB predicted from MD simulations to bind in the active site of pcDHFR. (a) Rotamer 1, (b) rotamer 2, (c) rotamer 3, and (d) rotamer 4.

requires a rotation about the N(2)–N(3) bond of the triazene linkage of 47° and steers the acetoxymethyl branch of TAB to within 3 \AA of Lys37 and permits a hydrogen bond between the acetoxymethyl oxygen and the Nz atom of Lys37.

Simulated Annealing Studies. To minimize operator bias, automated docking studies using simulated annealing were also investigated. The restricted rotation about the phenyl-pyrimidine linkage gives rise to two families of conformations (atropisomers). In one, the torsion angle between the two rings is about 60° , and in the other, it is about -50° (Table 2). As a result the triazene unit interacts with residues either above or below the plane of the 2,4-diaminopyrimidine. Each of these families is further split into two by the restricted rotation about the bonds each side of the N(1)=N(2) double bond ("crankshaft" motions).

Each of the four low-energy conformations of the ligand (Figure 4) can be accommodated within the active site (Figure 5). In rotamer 1, the acetoxymethyl branch is accommodated in the hydrophobic pocket formed by residues Ile33, Phe36, Phe69, Leu72, and Arg75, similar to that observed in the crystal structure (Figure 5a). Compared to the starting conformation of TAB before the dynamics run, the "crankshaft" rotation along the entire triazene linkage did not alter significantly the position of the benzyl and the acetoxymethyl function. The benzyl function adopts a face-edge orientation with Pro66 and Phe69. The guanidino group of Arg75 is within reach of the carbonyl oxygen and can establish a hydrogen bond. The bond linking the 5-phenyl group to the triazene linkage deviates out of plane only slightly (14°). In rotamer 2, there is a stacking interaction between the benzyl substituent of TAB and Phe69 (Figure 5b). The methylene linker establishes hydrophobic contact with Phe36 as a result of rotation along the N(2)–N(3) triazene bond by around 180° compared to the starting structure of TAB. This rotation directs the acetoxymethyl group toward the opening of the binding site cleft, allowing the ester oxygen and the

ethylene linkage to establish contact with Ile65 and Pro66, respectively. The methyl moiety of the acetoxymethyl group also makes contact with Phe69.

In rotamer 3 (Figure 5c), compared with rotamer 1, there is a 150° rotation about the torsion angle along the N(2)–N(3) bond, making it 28° out of plane (Table 2). The benzyl group of TAB establishes a hydrophobic contact with Ile33 and Pro66, and a distant face-edge conformation is established with Phe69; the acetoxymethyl group is within range of forming a charge-mediated hydrogen bond with Lys28. In rotamer 4 (Figure 5d) rotation about the N(2)–N(3) bond (33°) places the benzyl function in the mouth of the active site cleft and the only obvious interaction is with Leu25, while the acetoxymethyl group lies inside the pocket formed by Ile33, Phe36, Pro66, and Phe69.

In the rotamer 1 complex, the total molecular mechanics energy of the pcDHFR–TAB–NADPH system is $-419.8 \text{ kcal mol}^{-1}$, while in the rotamer 2 complex this value is $-429.2 \text{ kcal mol}^{-1}$. The rotamer 3 and rotamer 4 complexes are predicted to be less favorable, having total energies of -401.2 and $395.5 \text{ kcal mol}^{-1}$, respectively.

DISCUSSION

TAB is a flexible molecule with a number of freely rotatable bonds. The conformers of TAB observed in the crystal structure of pcDHFR in complex with NADPH correspond closely to two of the models produced from molecular dynamics runs (rotamers 1 and 2) which also reproduce accurately the orientation of several important active site residues such as Phe36, Thr61, Phe69, and Leu72, as well as the benzyl moiety of TAB. There are some regions of the backbone conformation that differ from that observed in the crystal structure. These differences are primarily in the external loop regions (i.e., near residues 23–26, 82–

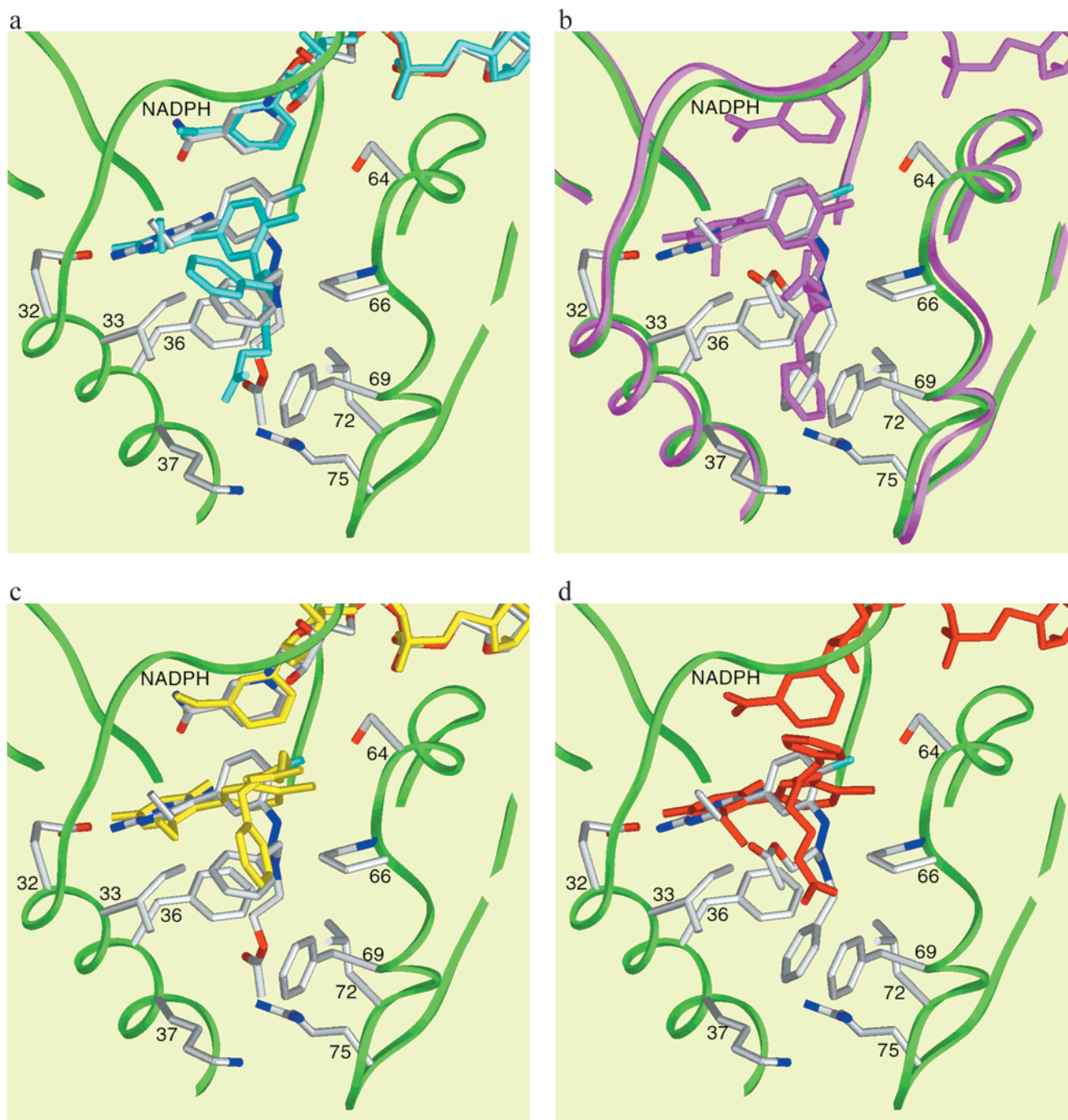


FIGURE 5: (a–d) Comparison of the conformations of TAB derived from dynamics studies with the crystal structure of pcDHFR complex. The pcDHFR crystal structure backbone is shown as a ribbon (green) with the TAB conformers and NADPH molecules with heteroatoms colored O (red), N (blue), P (yellow), and Cl (cyan). (a) rotamer 1 (cyan), (b) ribbon diagram for MD pcDHFR and rotamer 2 (violet), (c) rotamer 3 (yellow), and (d) rotamer 4 (red). SETOR program used to create figure (41).

93, 108–113, and 180–185) and likely reflect solvent termination effects in the MD calculations. The position of the cofactor NADPH from MD calculations is also consistent with X-ray data. The inter-ring torsional angle about the pyrimidine–phenyl bond is found to be similar to the crystal structure (52° , cf. 60°). Despite a close match for the benzyl substituent, the crystallography reveals that the acetyloxy branch does not forge any contact with Lys37 as predicted in the manual docking study. Instead, hydrophobic interactions are established with Ile33 and Phe36. Unlike Phe69, which is located deep in the active site, Lys37 is on the surface of the active-site cleft. The flexible nature of this

side chain, as well as the freely rotatable acetyloxy group inevitably makes prediction difficult. In the crystal structure, TAB is buried slightly deeper in the active site by approximately $1.35\text{--}2\text{ \AA}$ than found for the MD studies. The carboxylate side chain of Glu32 with which TAB forms two hydrogen bonds is highly flexible. To prevent TAB from being “ejected” from the enzyme active site and the further loss of hydrogen bond contacts with Ile10 and Ile123 during simulated annealing runs using the “soft-repulsion” potential, distance restraints were imposed to preserve these interactions. The crystallographic results suggest that the force constant for these restraints was set too high to leave any

freedom for the pyrimidine moiety of TAB to optimize its interactions through lateral movements.

Since explicit solvent molecules were not included in the dynamics runs, a distance-dependent dielectric constant was introduced, first to mimic the polarization effect in attractive interactions (closer interactions are given a higher weighting) and second to provide electrostatic screening effects of solvent by damping longer range charge interactions more than the ones in the shorter range (42). However, hydrophobic effects and frictional forces due to van der Waals contacts between protein and solvent molecules cannot be modeled in this way. The latter fact is advantageous to us, as inclusion of water molecules would have impeded the freedom of TAB to explore conformational space during dynamics simulations. The active site of pcDHFR is lined with hydrophobic residues with Lys37 and Arg75 being the exception. It is conceivable that solvent molecules may interact with the triazenyl linkage of TAB and/or the acetoxy branch to establish solvent-mediated hydrogen bonds with other active-site enzyme residues. However, the crystal structure data suggests that this is not the case. The role of water molecules in protein–ligand interactions is a complex phenomenon (43). For loosely bound solvent, their replacement by TAB upon binding to the enzyme active site will involve both entropic (release of water molecules to bulk solvent) and enthalpic factors (favorable interactions with other water molecules). Due to the qualitative nature of the dynamic calculations, it is beyond the scope of this study to access the influence of solvents on various enthalpic and entropic contributions to the protein–ligand complex.

The orientations of TAB observed in rotamers 3 and 4 are only seen in the molecular dynamics simulations. When the bulky triazenyl substituents interact with residues below the plane of the 2,4-diaminopyrimidine ring such as Leu25 and Lys28, there are no obvious favorable interactions that can be established as they are not buried deep into the active site but close to the surface of the cleft and would be subjected to the effects of solvent. The reduction in the number of interactions between the substituted triazenyl groups in rotamers 3 and 4 and the enzyme amino acid residues have translated to an increase in binding energy, making these binding orientations enthalpically less favorable.

Although manual docking studies can locate likely interaction geometries, an exhaustive and unbiased search is not feasible by this method. Therefore, a series of molecular dynamics runs utilizing a simulated annealing technique with a soft repulsion term has been performed to allow the exploration of the conformational space that TAB can adopt when bound to pcDHFR. These results illustrate the value of molecular dynamics runs, utilizing the simulated annealing technique with a soft repulsion term, for the exploration of the conformational space that TAB can adopt when bound to pcDHFR (44). To allow TAB to reach the alternative binding conformations, ligand side chains must be able to “pass through” enzyme amino acids residues without excessive energetic penalties. Replacing the van der Waals and electrostatic terms with a soft repulsion one, the energy between two nonbonded atoms remains finite even if their interatomic distance is zero. The different bound conformations are then interconvertible when simulated annealing is performed at temperatures that do not excessively distort the bonded geometry.

TAB can exist in four rotational isomeric forms separated by relatively high barriers due to restricted rotation about the pyrimidine–phenyl and N(2)–N(3) bonds. Rotation of the bond linking the 5-phenyl group to the triazenyl chain will result in the generation of more isomers. However, these latter “crankshaft” motions produce only minor shifts in the locations of the distant benzyl and acetoxy moieties. Restricted internal rotation is a feature of aryl-3,3-disubstituted triazenes, which results from the partial double bonded character of the N(2)–N(3) bond (10, 15, 16). Also the atropisomerism dictated by rotational restriction of the pyrimidine–phenyl bond is analogous to the restricted rotation of *o*-substituted biphenyls (17, 18). Results from molecular dynamics studies suggested that each of the resulting rotational isomeric forms might be accommodated in the active site of pcDHFR. Though two of the rotameric forms were more favorable than the other two, crystallographic results suggest that this energy penalty is decisive. All orientations for TAB differ somewhat from those observed for less bulky DHFR inhibitors. The bulky triazene substituent of TAB cannot occupy the binding pocket in the same way that methylbenzoprim **5** binds to the *Lactobacillus casei* enzyme (20) due to steric clashes with the cofactor. When TAB is forced to adopt such an orientation, the triazene subunit is pushed toward the opening of the binding cleft, thus, interacting unproductively with surface water molecules. This alternative rotameric form loses the hydrophobic interactions that are predicted to favor binding to pcDHFR—namely the face–edge interaction between the benzyl function of TAB and Phe69.

Overall, the acetoxyethyl and benzyl moiety of TAB can establish particularly strong hydrophobic interactions with enzyme residues such as Ile33, Phe36, Phe69, Leu72, and Arg75. The failure to observe conformations in which the triazene unit is directed toward the nicotinamide pocket may, in part, reflect the bulk of the triazene substituents and so the likelihood of severe steric clashes.

Improvement of species selectivity and potency is envisaged by further modification of the TAB anti-pcDHFR structure. For example, lengthening of the ethylene branch of TAB attached to the terminal triazenyl nitrogen should place the carbonyl oxygen of the acetoxy group closer to Lys37 for hydrogen bond formation; replacement of the benzyl function of TAB with a naphthalenemethyl group to maximize aromatic–aromatic interactions. It is envisioned that Lys37 and Phe69 are potential targets for selective DHFR inhibitors against pcDHFR.

REFERENCES

1. Mills, J. *Rev. Infect. Dis.* (1986) 8, 1001–1011.
2. Kovacs, J. A., Hiemenz, J. W., Macher, A. M., Stover, D., Murray, H. W., Shelhamer, J., Lane, H. C., Urmacher, C., Honig, C., Longo, D. L., Parker, M. M., Natanson, C., Parrillo, J. E., Fauci, A. S., Pizzo, P. A., and Masur, H. (1984) *Ann. Intern. Med.* 100, 663–671.
3. Kovacs, J. A., and Masur, H. (1988) *J. Infect. Dis.* 158, 254–259.
4. Queener, S. F., Bartlett, M. S., Jay, M. A., Durkin, M. M., and Smith, J. W. (1987) *Antimicrob. Agents Chemother.* 31, 1323–1327.
5. Queener, S. F. (1995) *J. Med. Chem.* 38, 4739–4759.
6. Piper, J. R., Johnson, C. A., Krauth, C. A., Carter, R. L., Hosmer, C. A., Queener, S. F., Borotz, S. E., and Pfefferkorn, E. R. (1996) *J. Med. Chem.* 39 (9) 1271–1280.

7. Rosowsky, A., Forsch, R. A., and Queener, S. F. (1995) *J. Med. Chem.* 38, 2615–2620.
8. Gangjee, A., Zhu, Y., Queener, S. F., Francom, P., and Broom, A. D. (1996) *J. Med. Chem.* 39, 1836–1845.
9. Gangjee, A., Guo, X., Queener, S. F., Cody, V., Galitsky, N., Luft, J. R., and Pangborn, W. (1998) *J. Med. Chem.* 41, 1263–1271.
10. Stevens, M. F. G., Phillip, K. S., Rathbone, D. L., O'Shea, D. M., Queener, S. F., Schwalbe, C. H., and Lambert, P. A. (1997) *J. Med. Chem.* 40, 1886–1893.
11. PDB files obtained from Protein Database (National Brookhaven Laboratories): 1DYR and 1DLS. Bernstein, F. C., Koetzle, T. F., Williams, G. J. B., Meyer, E. F., Brice, M. D., Rodgers, J. R., Kennard, O., Shimanouchi, T., and Tasumi, M. (1977) *J. Mol. Biol.* 112, 535–542.
12. Gschwend, D. A., Sirawaraporn, W., Santi, D. V., and Kuntz, I. D. (1977) *Proteins: Struct., Funct., Genet.* 29, 59–67.
13. Gschwend, D. A., Good, A. C., and Kuntz, I. D. (1996) *J. Mol. Recognit.* 9, 175–186.
14. Gorse, A. D., and Gready, J. E. (1997) *Protein Eng.* 10, 23–30.
15. Akhtar, M. H., Feser, M., and Oehlschlager, A. C. (1968) *Tetrahedron* 24, 3899–3906.
16. Hooper, D. L., Pottie, I. R., Vacheresse, M., and Vaughan, K. (1998) *Can. J. Chem.* 76, 125–135.
17. Wolf, C., König, W. A., and Roussel, C. (1995) *Libigs Ann. Chem.* 781–786.
18. Meyer, W. L., and Meyer, R. B. (1963) *J. Am. Chem. Soc.* 85, 2170–2171.
19. Tendler, S. J. B., Griffin, R. J., Birdsall, B., Stevens, M. F. G., Roberts, G. C. K., and Feeney, J. (1988) *FEBS Lett.* 240, 201–204.
20. Birdsall, B., Tendler, S. J. B., Feeney, A. J., Griffin, R. J., Carr, M. D., Thomas, J. A., Roberts, G. C. K., and Stevens, M. F. G. (1990) *Biochemistry* 29, 9660–9667.
21. Champness, J. N., Achari, A., Ballantine, S. P., Byrant, P. K., Delves, C. J., and Stammers, D. K. (1994) *Structure* 2, 915–924.
22. Cody, V., Galitsky, N., Rak, D., Luft, J. R., Pangborn, W., and Queener, S. F. (1999) *Biochemistry*, 38, 4303–4312.
23. Cody, V., Galitsky, N., Luft, J. R., Pangborn, W., Gangjee, A., Devraj, R., Queener, S. F., and Blakley, R. L. (1997) *Acta Crystallogr., Sect. D* 53, 638–649.
24. Broughton, M. C., and Queener, S. F. (1991) *Antimicrob. Agents Chemother.* 35, 1348–1355.
25. DeTitta, G. T., Dembik, D. M., Pangborn, W. A., and Luft, J. R. (1996) *Acta Crystallogr., Sect. A* 52, C504.
26. Luft, J. R., Rak, D. M., DeTitta, G. T. (1999) *J. Cryst. Growth* 196, 447–449, 450–455.
27. Hendrickson, W. A., and Konnert, J. H. (1980) Indian Academy of Sciences: Bangalore, India.
28. Finzel, B. C. (1987) *J. Appl. Crystallogr.* 20, 53.
29. Sack, J. S. (1988) *J. Mol. Graphics* 6, 244–245.
30. SYBYL Molecular Modeling Package, version 6.0; Tripos, St. Louis, MO, 1997.
31. Laskowski, R. A., MacArthur, M. W., Moss, D. S., and Thornton, J. M. (1993) *J. Appl. Crystallogr.* 26, 283–291.
32. Steward, J. J. P. (1990) *J. Comput. Aided Mol. Des.* 4, 1–105.
33. Dewar, M. J., Zebisch, E. G. S., Healy, E. F., and Stewart, J. J. P. (1985) *J. Am. Chem. Soc.* 107, 3902–3909.
34. Besler, B. H., Merz, K. M., and Kollman, P. A. (1989) *J. Comput. Chem.* 11, 431–739.
35. INSIGHT II (1995) Molecular Simulations, San Diego.
36. Weiner, S. J., Kollman, P. A., Nguyen, D. T., and Case, D. A. (1986) *J. Comput. Chem.* 7, 230–252.
37. Pearlman, D. A. (1995) AMBER 4.1; University of California, San Francisco, CA.
38. Cornell, W. D., Cipplak, P., Bayly, C. I., Gould, I. R., Merz, K. M., Jr., Ferguson, D. M., Spellmeyer, D. C., Fox, T., Caldwell, J. W., and Kollman, P. A. (1995) *J. Am. Chem. Soc.* 117, 5179–5197.
39. Leach, A. R., and Klein, T. E. (1985) *J. Comput. Chem.* 11, 1379–1393.
40. Ryckaert, J., Ciccotti, G., and Berendsen, H. (1977) *J. Comput. Phys.* 23, 327–341.
41. Evans, S. V. (1993) *J. Mol. Graphics* 11, 134–138.
42. Weiner, S. J., Kollman, P. A., Case, D. A., Singh, U. C., Ghio, C., Alagona, G., Profeta, S., Jr., and Weiner, P. (1984) *J. Am. Chem. Soc.* 106, 765–784.
43. Blokzijl, V. W., and Engberts, J. B. F. N. (1993) *Angew. Chem., Int. Ed. Engl.* 32, 1545–1579.
44. Laughton, C. A. (1994) *Protein Eng.* 7, 235–241.

BI9924563